RSC Advances

PAPER

View Article Online
View Journal | View Issue

Cite this: *RSC Adv.*, 2014, **4**, 43131

Cs-substituted tungstophosphate-supported ruthenium nanoparticles as efficient and robust bifunctional catalysts for the conversion of inulin and cellulose into hexitols in water in the presence of H_2†

Weiping Deng, Enze Zhu, Mi Liu, Qinghong Zhang and Ye Wang*

Received 19th June 2014
Accepted 1st September 2014

DOI: 10.1039/c4ra05939e

www.rsc.org/advances

Cellulose and inulin, two important biomasses, can be transformed to polyols using bifunctional catalysts combining acid sites for hydrolysis and metal nanoparticles for hydrogenation. Here, we report that Ru nanoparticles loaded on a Keggin-type polyoxometalate, *i.e.*, $Cs_3PW_{12}O_{40}$, without intrinsic Brønsted acidity exhibit superior catalytic performances for the transformation of inulin and cellulose into hexitols in water in the presence of H_2. We demonstrated that new Brønsted acid sites were generated from H_2 on the $Ru/Cs_3PW_{12}O_{40}$ catalyst. The H_2-originated reversible Brønsted acid sites were robust during the transformation of biomass under hydrothermal conditions. We further found that the mean size of Ru nanoparticles determined the product selectivity in the conversion of inulin under H_2. The catalyst with larger Ru nanoparticles favoured the formation of fructose, the hydrolysis product, while the major products were hexitols over the catalyst with a smaller Ru particle size. We clarified that, as compared to that of inulin hydrolysis, the rate of fructose hydrogenation increased more rapidly upon decreasing the Ru particle size.

1. Introduction

Cellulose is a polymer of D-glucose linked by β-1,4-glycosidic bonds (Scheme 1) and is a major component of the abundant and inedible lignocellulosic biomass. The catalytic transformation of cellulose into chemicals or fuels has attracted much attention in recent years from the viewpoint of establishing sustainable chemical and energy processes.[1] Because of the huge numbers of hydroxyl groups and the linkage of β-1,4-glycosidic bonds, extensive hydrogen-bonding networks exist in cellulose macromolecules, making their crystalline structure highly robust. The catalytic transformation of cellulose under mild conditions is a difficult task.

On the other hand, inulin is also a non-digestible carbohydrate composed of linear β-2,1-linked fructose chains with a terminal glucopyranose unit (Scheme 1). Generally, inulin amounts to 70–90 wt% of Jerusalem artichoke, which is a perennial plant and can grow in wide range of ecological conditions.[2] To date, only a few studies have been devoted to the catalytic transformation of inulin into chemicals and fuels

State Key Laboratory of Physical Chemistry of Solid Surfaces, Collaborative Innovation Center of Chemistry for Energy Materials, National Engineering Laboratory for Green Productions of Alcohols, Ethers and Esters, College of Chemistry and Chemical Engineering, Xiamen University, China. E-mail: wangye@xmu.edu.cn; Fax: +86 592 2183047; Tel: +86 592 2186156

† Electronic supplementary information (ESI) available: XRD patterns of $Cs_xH_{3-x}PW_{12}O_{40}$ and $Ru/Cs_xH_{3-x}PW_{12}O_{40}$; N_2 adsorption–desorption isotherms of $Cs_xH_{3-x}PW_{12}O_{40}$; XPS spectra for $Ru/Cs_xH_{3-x}PW_{12}O_{40}$ catalysts; TEM micrograph for colloidal Ru particles synthesized by the reduction of $RuCl_3$ with ascorbic acid; NH_3-TPD profiles of several solid acids; TEM micrographs for Ru nanoparticles loading on several solid acids; XRD patterns and XPS spectra for $Ru/Cs_3PW_{12}O_{40}$ before and after reaction; pyridine-adsorption IR for $Cs_3PW_{12}O_{40}$ and Ru/Al_2O_3 under different H_2 pressures; Raman spectra of $Cs_3PW_{12}O_{40}$ under H_2 and N_2; TEM micrographs of Ru nanoparticles with different mean sizes; hydrogenation of fructose over $Ru/Cs_3PW_{12}O_{40}$ with different mean sizes of Ru nanoparticles and the corresponding turnover frequencies for these catalysts. See DOI: 10.1039/c4ra05939e

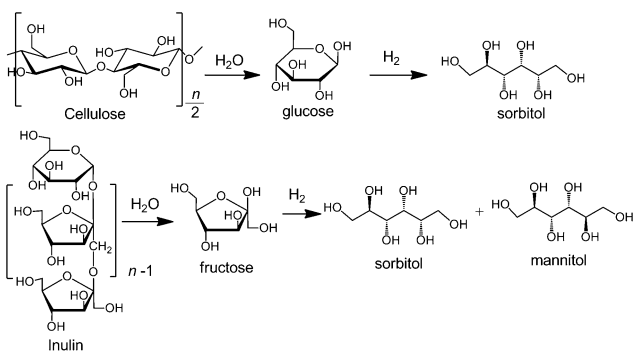

Scheme 1 Catalytic conversions of cellulose and inulin into hexitols *via* hydrolysis and hydrogenation.

under mild conditions.[3,4] Moreover, there are various C–C and C–O bonds in both inulin and cellulose macromolecules. The selective cleavage of specific chemical bonds in inulin or cellulose to form a specific product is also a challenging research theme.

The production of hexitols including sorbitol and mannitol is one of the most attractive routes for the utilization of biomass resources. Both sorbitol and mannitol find many applications in food, pharmaceutical, and cosmetic industries. Sorbitol is also regarded as one of the top value-added chemicals from biomass for the production of isosorbide, 1,4-sorbitan, 2,5-anhydrosugars, lactic acid, glycerol, ethylene glycol, and propylene glycol.[5] For the production of hexitols from a biomass such as cellulose or inulin, a bifunctional catalyst or catalytic system that combines the hydrolysis and hydrogenation functions is generally required. Liu and co-workers developed an intriguing bifunctional system, which combined the reversibly generated H_3O^+ in hot water (518 K) with a hydrogenation catalyst, *i.e.*, Ru/activated carbon (AC), for the conversion of cellulose to hexitols with a yield approaching 40%.[6] The combination of a liquid mineral acid (*e.g.*, HCl and H_2SO_4) with a supported Ru or Pt catalyst was further demonstrated to be highly efficient for the selective conversion of cellulose into hexitols under mild conditions.[7] Although excellent performances have been achieved by using these systems containing a liquid acid, the problems of the recovery of the liquid acid and the corrosion of the reactor would hinder the application of these systems for large-scale production.

Bifunctional catalysts based on solid acid-supported metal nanoparticles have also attracted much attention for the transformation of cellulose in recent years. Fukuoka and Dhepe reported a pioneering work on the conversion of cellulose in water and obtained a hexitol yield of 31% over a Pt/γ-Al_2O_3 catalyst at 463 K under H_2 atmosphere.[8] We also demonstrated that Ru nanoparticles supported on carbon nanotubes (CNTs) bearing oxygen-containing functional groups, which could work as acid sites, were efficient for the conversion of cellulose and cellobiose, a glucose dimer also connected by β-1,4-glycosidic bond, into hexitols.[9] Carbon-supported nickel or nickel phosphide catalysts could also catalyze the conversion of cellulose into sorbitol under proper conditions.[10]

On the other hand, the studies on the catalytic conversion of inulin to hexitols in water under H_2 atmosphere are scarce. Heinen *et al.* demonstrated that a homogeneous Ru catalyst (Ru–P(*m*-$C_6H_4SO_3Na)_3$) in combination with HCl catalyzed the production of mannitol from inulin. However, after reaction under H_2 atmosphere at 363 K, the homogeneous Ru catalyst was reduced and became precipitated.[3a] An acidified active carbon supported-Ru catalyst was claimed to be also efficient and more stable for the transformation of inulin into hexitols at 373 K.[3b] A Ni–W_2C/AC catalyst with C–C bond cleavage ability could catalyze the direct conversion of Jerusalem artichoke to 1,2-propylene glycol with a yield of 35%.[4]

In short, although some bifunctional heterogeneous catalysts have been reported for the conversion of cellulose or inulin, the catalytic efficiency and catalyst stability are still unsatisfactory. The development of robust solid acid materials or systems capable of working under hydrothermal conditions remains highly challenging.

Polyoxometalates, particularly the Keggin-type heteropolyacids, have recently attracted much attention for the catalytic hydrolysis of cellulose because of their strong Brønsted acidity.[11,12] The combination of $H_3PW_{12}O_{40}$ or $H_4SiW_{12}O_{40}$ with Ru/C could catalyze the transformation of cellulose into hexitols with good yields.[13] However, the Keggin-type heteropolyacids are soluble in water and cannot be used as heterogeneous catalysts for the transformation of biomass in water. It was once claimed that the $H_3PW_{12}O_{40}$ incorporated inside the mesoporous cavities of metal–organic frameworks (MOFs) worked as a heterogeneous catalyst for the conversion of cellulose in water, but this catalyst could not be used recyclably.[14] The salts of heteropolyacids with larger monovalent cations such as Cs^+ are insoluble. Moreover, the H-form Cs salts of Keggin-type heteropolyacids with proper Cs contents may possess reasonably large surface areas and mesoporosity due to the stacking of primary particles.[15] Thus, the Cs salts of Keggin-type heteropolyacids may work as water-tolerant solid-acid catalysts.[15] A few studies have reported the utilization of $Cs_xH_{3-x}PW_{12}O_{40}$ or $Cs_xH_{4-x}SiW_{12}O_{40}$ for the transformation of cellulose. For example, the combination of $Cs_{2.5}H_{0.5}PW_{12}O_{40}$ or $Cs_{3.5}H_{0.5}$-$SiW_{12}O_{40}$ with Ru/C was found to be highly efficient for the conversion of cellulose to hexitols in water under H_2 atmosphere.[16] However, the leaching of tungsten species was observed during the reaction.[16]

In a short communication, we demonstrated that Ru nanoparticles loaded on Cs salts of tungstophosphoric acid, *i.e.*, $Cs_xH_{3-x}PW_{12}O_{40}$, were efficient bifunctional catalysts for the transformations of cellobiose, the model molecule of cellulose, into sorbitol.[17] We observed the leaching of H^+-rich hydrophilic moiety into H_2O under hydrothermal reaction conditions. Unexpectedly, the Ru/$Cs_3PW_{12}O_{40}$ without intrinsic Brønsted acidity could catalyze the conversion of cellobiose to sorbitol in the presence of H_2. In the present paper, we report our recent comprehensive studies on the transformations of inulin and cellulose in H_2O under H_2 over polyoxometalate-supported Ru catalysts. We focus on the catalytic behaviours and functioning mechanisms of the Ru/$Cs_3PW_{12}O_{40}$ catalyst and the origin of the acidity for this catalyst. The size effect of Ru nanoparticles will be discussed. Our present work provides a novel strategy for the design of stable bifunctional catalysts for the transformation of biomass under H_2 atmosphere under hydrothermal conditions.

2. Experimental section

2.1 Catalyst preparation

The Cs salts of tungstophosphates with different Cs contents ($Cs_xH_{3-x}PW_{12}O_{40}$, x = 1.0–3.0) were prepared by a reaction between $H_3PW_{12}O_{40}$ and Cs_2CO_3. The precipitates obtained after the addition of the aqueous solution of Cs_2CO_3 into that of $H_3PW_{12}O_{40}$ were recovered by filtration, followed by washing with deionized water, drying, and calcination to obtain the $Cs_xH_{3-x}PW_{12}O_{40}$ samples. As an example, for the synthesis of $Cs_3PW_{12}O_{40}$, the aqueous solution of Cs_2CO_3 with a

concentration of 0.02 mol L^{-1} (150 mL) was added into that of $H_3PW_{12}O_{40}$ with a concentration of 0.12 mol L^{-1} (15 mL). Then, the recovered precipitate was calcined in air at 673 K for 2 h after washing and drying.

The controlled syntheses of colloidal Ru nanoparticles with mean sizes ranging from 1.6 to 10.8 nm were performed by the reduction of $RuCl_3$ with ascorbic acid in H_2O, ethylene glycol, or butylene glycol at different temperatures and aging times. The detailed synthetic conditions will be described later. The Ru/$Cs_xH_{3-x}PW_{12}O_{40}$ catalysts were prepared by an adsorption of the colloidal Ru nanoparticles onto the $Cs_xH_{3-x}PW_{12}O_{40}$ samples. In brief, $Cs_xH_{3-x}PW_{12}O_{40}$ white powders (1.0 g) were added into 20 mL aqueous solution containing the colloidal Ru nanoparticles (Ru weight, 10 mg). The addition of the polyoxometalate powders decoloured the solution, while the colour of the support was deepened, indicating the occurrence of the adsorption of colloidal Ru nanoparticles onto the support. After filtration, washing with deionized water, and drying at 373 K, the Ru/$Cs_xH_{3-x}PW_{12}O_{40}$ catalysts were obtained. The same adsorption procedure was also employed for the preparation of Ru nanoparticles loaded on other solid acid supports. The loading of Ru was kept at 1.0 wt% in each catalyst.

2.2 Catalyst characterization

Powder X-ray diffraction (XRD) patterns were collected on a Panalytical X'Pert Pro Super X-ray diffractometer equipped with X'Celerator detection. The Cu K_α radiation (40 kV and 30 mA) was used as the X-ray source. X-ray photoelectron spectra (XPS) were recorded with a Quantum 2000 Scanning ESCA Microprobe instrument (Physical Electronics) using Al K_α radiation. The binding energy was calibrated using C_{1s} photoelectron peak at 284.6 eV as a reference. Transmission electron microscopy (TEM) measurements were performed on a JEM-2100 electron microscope operated at an acceleration voltage of 200 kV. The mean size of Ru nanoparticles in the sample was estimated from the TEM micrographs by counting around 150–200 particles.

The CO chemisorption was measured with a Micromeritics ASAP 2010C instrument. The acidity of the catalyst was examined by ammonia temperature-programmed desorption (NH_3-TPD) and pyridine-adsorbed Fourier-transform infrared (FT-IR) studies. NH_3-TPD was performed on a Micromeritics AutoChem 2920 II instrument. Typically, the sample loaded in a quartz reactor was pretreated with high-purity He at 623 K for 1 h. After the sample was cooled down to 373 K, the adsorption of NH_3 was performed by switching the He flow to a NH_3–He (10 vol% NH_3) gas mixture and then maintaining the sample at 373 K for 0.5 h. The gas phase and weakly adsorbed NH_3 molecules were purged by high-purity He at the same temperature. NH_3-TPD was then performed in the He flow by raising the temperature to 1073 K at a rate of 10 K min^{-1}. The desorbed NH_3 molecules were detected by using a ThermoStar GSD 301 T2 mass spectrometer with the signal of m/z of 16.

Pyridine-adsorbed FT-IR was performed with a Nicolet Avatar 330 instrument equipped with an MCT detector with a resolution of 4 cm^{-1}. The sample was pressed into a self-supported wafer, and placed in an *in situ* IR cell. After pretreatment in H_2 at 573 K, followed by evacuation at the same temperature, the sample was cooled down to 423 K and was exposed to pyridine for 0.5 h. After cooling down to 303 K followed by a brief evacuation to remove the gaseous pyridine, H_2 or N_2 was introduced. FT-IR spectra were recorded under H_2 or N_2 with different pressures. The Raman spectra were collected on a Renishaw Raman System 1000 spectrometer. Electron spin resonance (ESR) spectroscopic experiments were carried out on a Bruker EMX-10/12 operating at X-band frequency of 9.43 GHz, modulation amplitude of 10.0 G, and modulation frequency of 100.0 kHz.

2.3 Catalytic reaction

The conversion of inulin or cellulose was performed with a batch-type high-pressure autoclave reactor. Typically, the catalyst and the reactant (inulin or cellulose) were added into a Teflon-lined stainless-steel reactor pre-charged with H_2O. Then, the reaction was carried out at 363 or 433 K under 2 MPa H_2 for 4 h or 24 h. After the reaction, the solid catalyst was separated by centrifugation, and the liquid products were analyzed by a HPLC (Shimazu LC-20A) equipped with a RI detector and a Shodex SUGARSC-1011 column (7 μm, 8 × 300 mm). The eluent was water with a flow rate of 0.5 cm^3 min^{-1}.

3. Results and discussion

3.1 Structures and physicochemical properties of $Cs_xH_{3-x}PW_{12}O_{40}$-supported Ru nanoparticles

The crystalline structures of the synthesized $Cs_xH_{3-x}PW_{12}O_{40}$ samples with different Cs contents (x = 1.0–3.0) were investigated by the XRD measurements (Fig. S1†). The XRD patterns for all the samples can be attributed to the cubic crystalline structure of Keggin-type polyoxometalate compounds.[18,19] The loading of Ru nanoparticles onto the $Cs_xH_{3-x}PW_{12}O_{40}$ (x = 1.0–3.0) samples did not significantly change the XRD patterns, suggesting that the crystalline structure was sustained (Fig. S1b†). N_2 physisorption studies revealed that the surface areas of the Ru/$Cs_xH_{3-x}PW_{12}O_{40}$ catalysts increased with increasing the Cs content from x = 1.0 to x = 3.0 (Table 1). The surface areas of the $Cs_xH_{3-x}PW_{12}O_{40}$ also increased in a similar trend with increasing the Cs content. The N_2 adsorption–desorption isotherms for the $Cs_xH_{3-x}PW_{12}O_{40}$ showed that the samples with higher Cs contents ($x \geq 2$) exhibited the type-IV isotherm, in which the hysteresis of desorption branch was clearly observed (Fig. S2†). This confirms that the substitution of the smaller H^+ with the larger Cs^+ in the polyoxometalate causes the formation of micropores and mesopores.[19]

NH_3-TPD measurements were performed to investigate the acidities of the Ru/$Cs_xH_{3-x}PW_{12}O_{40}$ catalysts. As displayed in Fig. 1, a major desorption peak at 850–855 K was observed for the catalyst with x < 3.0. This peak could be ascribed to the desorption of NH_3 from the strong acid sites, which are believed to be the Brønsted acid sites, over the Keggin-type polyoxometalates.[19] As expected, no desorption of NH_3 was observed for the Ru/$Cs_3PW_{12}O_{40}$ catalyst. We have quantified the amount of NH_3 desorption using the peak at 850–855 K, and the result is

Table 1 Some physicochemical properties of $Ru/Cs_xH_{3-x}PW_{12}O_{40}$ catalysts

Catalyst	Surf. area ($m^2\ g^{-1}$)	NH_3 desorption amount[a] (mmol g^{-1})	D(Ru)[b]	d(Ru)[c] (nm)
$Ru/Cs_{1.0}H_{2.0}PW_{12}O_{40}$	59	117	n.d.[d]	—
$Ru/Cs_{1.5}H_{1.5}PW_{12}O_{40}$	60	92	0.47	1.9
$Ru/Cs_{2.0}H_{1.0}PW_{12}O_{40}$	76	83	0.45	2.0
$Ru/Cs_{2.5}H_{0.5}PW_{12}O_{40}$	93	37	n.d.[d]	—
$Ru/Cs_{3.0}PW_{12}O_{40}$	98	0	0.49	1.8

[a] Quantified from NH_3-TPD. [b] D(Ru) denotes the Ru dispersion obtained from CO chemisorption. [c] d(Ru) denotes the size of Ru particles estimated from D(Ru) by using $d(\mathrm{Ru}) = 6V_m/[D(\mathrm{Ru}) \times a_m]$ (nm).[20] [d] Not detected.

displayed in Table 1. The amount of NH_3 desorption decreased gradually with increasing the Cs content, becoming zero at $x = 3.0$. No Brønsted acid sites exist on the $Ru/Cs_3PW_{12}O_{40}$ catalyst.

XPS studies were performed to gain information on the chemical state of Ru over our catalysts. The result showed that the binding energies of Ru $3d_{5/2}$ were at ~280.4 eV for the $Ru/Cs_xH_{3-x}PW_{12}O_{40}$ catalysts with different Cs contents (Fig. S3†). This suggests that the Ru species are all in metallic state over these catalysts. We have performed TEM measurements for the $Ru/Cs_xH_{3-x}PW_{12}O_{40}$ catalysts. However, we failed to distinguish the Ru nanoparticles from the $Cs_xH_{3-x}PW_{12}O_{40}$ supports in the TEM images possibly because of the weak contrast between Ru and Cs. We measured the dispersion of Ru nanoparticles for several typical catalysts by the CO chemisorption technique. The dispersions of Ru, denoted as D(Ru), were quite similar (0.45–0.49) for these catalysts (Table 1). It is known that the size of metallic Ru particles, denoted as d(Ru), can be evaluated from the Ru dispersion. We have estimated the size of Ru particles by using the following relationship, $d(\mathrm{Ru}) = 6V_m/[D(\mathrm{Ru}) \times a_m]$ (nm), where D(Ru), V_m, and a_m are the Ru dispersion, the volume occupied by a metal atom in the bulk, and the surface area occupied by an exposed surface metal atom, respectively.[20] By using the V_m (13.65×10^{-3} nm^3) and a_m (9.09×10^{-2} nm^2) values reported in literature,[20] we obtained the sizes of Ru nanoparticles of 1.8–2.0 nm for the catalysts with Ru dispersions of 0.49–0.45 (Table 1). These size values are close to that of Ru nanoparticles (1.6 nm) in the colloids used for the preparation of the supported catalysts by an adsorption method (Fig. S4†).

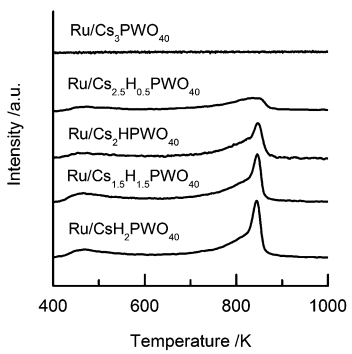

Fig. 1 NH_3-TPD profiles for the $Ru/Cs_xH_{3-x}PW_{12}O_{40}$ catalysts with different Cs contents.

3.2 Catalytic behaviours of polyoxometalates and polyoxometalate-supported Ru nanoparticles for the conversion of inulin

We first investigated the catalytic behaviours of the $Cs_xH_{3-x}PW_{12}O_{40}$ samples for the hydrolysis of inulin in water. Over the $Cs_xH_{3-x}PW_{12}O_{40}$ ($x = 1.0$–2.5) samples with strong Brønsted acidity, inulin could be completely converted at 363 K, and fructose was formed as a major product with a yield of 74–88% (Fig. 2). Glucose and sucrose were the main by-products. Glucose could be formed by the hydrolysis of the terminal glucopyranose or by the isomerization of fructose over the Lewis acid site on our catalyst, whereas sucrose may be produced *via* partial hydrolysis of inulin without breaking the linkage between terminal glucopyranose and fructose. The $Cs_3PW_{12}O_{40}$, which had no Brønsted acidity, showed very low inulin conversion and fructose yield (<5%). Such a low activity was probably due to the presence of weak Lewis acid sites on the $Cs_3PW_{12}O_{40}$. For comparison, the catalytic performances of several other typical solid acids are also displayed in Fig. 2. Al_2O_3 exhibited a low activity for the hydrolysis of inulin probably because of its relatively weaker acidity (Fig. S5 and Table S1†). In addition to fructose, glucose, sucrose and some oligomers were also formed over Al_2O_3. Zeolites HZSM-5 and MCM-22 bearing stronger acidities and larger densities of acid sites (Fig. S5 and Table S1†) showed higher fructose yields. Although HZSM-5 possessed stronger acidity than MCM-22, its activity for inulin hydrolysis was lower. This is probably due to the smaller

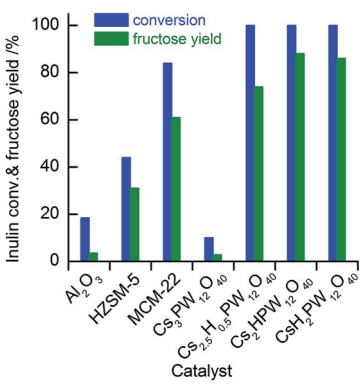

Fig. 2 Catalytic behaviours of the $Cs_xH_{3-x}PW_{12}O_{40}$ as well as some typical solid acids for the hydrolysis of inulin. Reaction conditions: inulin 0.20 g; catalyst, 0.050 g; H_2O, 10 mL; $T = 363$ K; $t = 4$ h.

pore size of HZSM-5 (Table S1†). The results in Fig. 2 demonstrate that the $Cs_xH_{3-x}PW_{12}O_{40}$ ($x < 3$) samples with strong Brønsted acidity catalyze the hydrolysis of inulin very efficiently, and the $Cs_3PW_{12}O_{40}$ is almost inactive for the hydrolysis reaction because of the lacking of Brønsted acidity.

Then, we investigated the catalytic performances of Ru nanoparticles loaded on the $Cs_xH_{3-x}PW_{12}O_{40}$ ($x = 1$–3) series of samples for the conversion of inulin in water under H_2 atmosphere. For comparison, Ru catalysts supported on other typical solid acids, *i.e.*, Al_2O_3, MCM-22, and HZSM-5, were also investigated (Table 2). All these supported Ru catalysts were prepared by the adsorption of colloidal Ru nanoparticles with a mean size of 1.6 nm onto the supports. The mean sizes of Ru particles over different supports were quite similar, being 1.6–2.3 nm (Fig. S6†). Catalytic studies showed that, in the absence of a catalyst (blank reaction), no inulin conversion was observed. As compared to the catalyst with Al_2O_3, MCM-22, or HZSM-5 as the support, polyoxometalate-supported Ru nanoparticles exhibited higher inulin conversions and higher hexitol (sorbitol and mannitol) yields. Hexitol yields of 79–84% were achieved over the $Ru/Cs_xH_{3-x}PW_{12}O_{40}$ catalysts for the conversion of inulin at 363 K for 4 h under a H_2 pressure of 2 MPa. The yield of sorbitol was roughly equal to that of mannitol over these catalysts. This is likely because fructose, the reaction intermediate, can be transformed equally into α- and β-form furans, which are then hydrogenated to form sorbitol and mannitol, respectively.[21] It is quite unexpected that the $Ru/Cs_3PW_{12}O_{40}$ catalyst, which does not possess intrinsic Brønsted acidity, shows the highest yield of hexitols (84%).

3.3 Catalytic behaviours of polyoxometalate-supported Ru nanoparticles for the conversion of cellulose

We have investigated the catalytic behaviours of the $Ru/Cs_xH_{3-x}PW_{12}O_{40}$ catalysts for the conversion of ball-milled cellulose in water under H_2 atmosphere. The catalytic conversion of cellulose provided hexitols, particularly sorbitol, as the major products. Under our reaction conditions, no hexitols were formed without a catalyst. The yields of hexitols over the $Ru/Cs_xH_{3-x}PW_{12}O_{40}$ catalysts were higher than those over the Ru nanoparticles loaded on Al_2O_3, H-ZSM-5, or H-MCM-22 (Fig. 3). The $Ru/Cs_3PW_{12}O_{40}$ catalyst without intrinsic Brønsted acidity was also efficient for the conversion of cellulose, providing a hexitol yield of 45% at 433 K. The $Ru/Cs_xH_{3-x}PW_{12}O_{40}$ catalysts with lower Cs contents ($x = 1.0$–2.0), which had strong Brønsted acidity, showed comparable or slightly higher hexitol yields than the $Ru/Cs_3PW_{12}O_{40}$. In other words, the presence of intrinsic Brønsted acid sites only contributed a little to the catalytic conversion of cellulose to hexitols.

We have examined the stability of the $Ru/Cs_3PW_{12}O_{40}$ and $Ru/Cs_2HPW_{12}O_{40}$ catalysts during the repeated uses for the conversion of ball-milled cellulose in water under H_2 at 433 K. The yields of hexitols decreased to some extent in the initial two recycles over both catalysts, and then remained stable in the next recycles (Fig. 4). However, the hexitol yield decreased more quickly over the $Ru/Cs_2HPW_{12}O_{40}$ catalyst than that over the $Ru/Cs_3PW_{12}O_{40}$ catalyst. Védrine and co-workers once reported that the $Cs_xH_{3-x}PW_{12}O_{40}$ might be composed of $Cs_3PW_{12}O_{40}$ with $H_3PW_{12}O_{40}$ dispersed in its pores, and the latter might be dissolved in hot water.[22] Okuhara *et al.* found that the treatment of $Cs_{2.5}H_{0.5}PW_{12}O_{40}$ in water at 393 K caused the leaching of H^+-rich hydrophilic moiety into water although they claimed that the protons were homogeneously dispersed in the $Cs_xH_{3-x}PW_{12}O_{40}$.[23] We also observed the leaching of H^+-rich hydrophilic moiety from the $Au/Cs_xH_{3-x}PW_{12}O_{40}$ catalysts for the oxidative transformation of cellulose under hydrothermal conditions.[24] Thus, we speculate that the leaching of H^+-rich hydrophilic moiety occurs for the $Ru/Cs_2HPW_{12}O_{40}$ catalyst. After four recycles, the hexitol yield over the $Ru/Cs_3PW_{12}O_{40}$ catalyst (41%) was slightly higher than that over the $Ru/Cs_2HPW_{12}O_{40}$ catalyst. From XRD, XPS and CO chemisorption measurements, we confirmed that the structure of the $Ru/Cs_3PW_{12}O_{40}$ catalyst did not undergo significant changes except for a slight increase in the size of Ru nanoparticles (Fig. S7 and Table S2†). The slight decrease in the activity of the $Ru/Cs_3PW_{12}O_{40}$ catalyst during the initial 2 recycles (Fig. 4) may be due to the increase in the size of Ru nanoparticles (Table S2†). Therefore, the $Ru/Cs_3PW_{12}O_{40}$ is a

Table 2 Catalytic performances of Ru nanoparticles loaded on polyoxometalates and other supports for the conversion of inulin in water under H_2[a]

		Yield[b] (%)				
Catalyst	Conv. (%)	Sor.	Man.	Fru.	Glu.	Suc.
Blank	0	0	0	0	0	0
Ru/Al_2O_3	6.1	0.9	0.8	0.7	0.4	1.1
Ru/HZSM-5	85	30	27	18	2.1	8.2
Ru/MCM-22	94	36	37	2.6	0.8	8.4
$Ru/Cs_{1.0}H_{2.0}PW_{12}O_{40}$	100	41	38	11	2.3	4.9
$Ru/Cs_{1.5}H_{1.5}PW_{12}O_{40}$	100	39	40	8.5	2.0	5.5
$Ru/Cs_{2.0}H_{1.0}PW_{12}O_{40}$	100	43	40	10	2.0	5.0
$Ru/Cs_{2.5}H_{0.5}PW_{12}O_{40}$	100	40	39	6.6	1.8	4.9
$Ru/Cs_{3.0}PW_{12}O_{40}$	100	43	41	4.9	2.1	6.0

[a] Reaction conditions: catalyst (Ru loading, 1.0 wt%), 0.05 g; inulin 0.2 g; H_2O, 10 mL; H_2, 2 MPa; $T = 363$ K; $t = 4$ h. [b] Sor., man., fru., glu., and suc. denote sorbitol, mannitol, fructose, glucose, and sucrose, respectively.

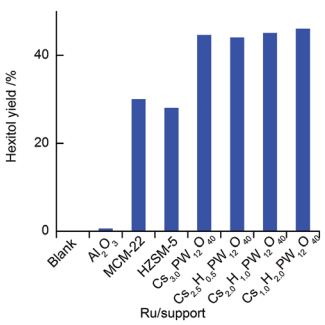

Fig. 3 Catalytic behaviours of Ru nanoparticles loaded on $Cs_xH_{3-x}PW_{12}O_{40}$ and several typical solid acids for the conversion of cellulose in water under H_2. Reaction conditions: cellulose (ball-milled), 0.10 g; catalyst, 0.10 g; H_2O, 10 mL; $T = 433$ K; $t = 24$ h.

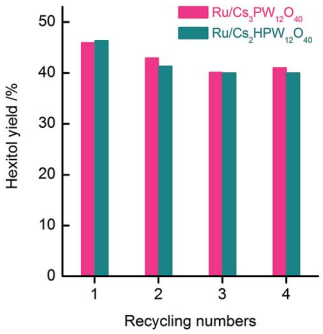

Fig. 4 Repeated uses of the $Ru/Cs_3PW_{12}O_{40}$ and $Ru/Cs_2HPW_{12}O_{40}$ catalysts for the conversion of cellulose in water under H_2. Reaction conditions: cellulose (ball-milled), 0.10 g; catalyst, 0.10 g; H_2O, 15 mL; H_2, 2 MPa; $T = 433$ K; $t = 24$ h.

highly efficient and relatively robust heterogeneous catalyst for the transformation of biomass (inulin and cellulose) under hydrothermal conditions.

3.4 Key factors determining the catalytic behaviour of $Ru/Cs_3PW_{12}O_{40}$ catalyst for the conversion of inulin

As described above, it is significant that the $Ru/Cs_3PW_{12}O_{40}$ catalyst without intrinsic Brønsted acidity shows superior catalytic performances for the production of hexitols from both inulin and cellulose. Taking inulin as an example, we have clarified that the H_2 pressure is one key factor determining the catalytic behaviour of this catalyst. Fig. 5 shows the effect of H_2 pressure on the conversion of inulin at 363 K. In the absence of H_2 (under 2 MPa N_2), the inulin conversion was only 20%, and the major product was fructose. The presence of H_2 significantly increased the inulin conversion; the inulin conversion increased from 20% to 97% by feeding H_2 with a low pressure (0.2 MPa) (Fig. 5). It is of interest that the yield of fructose, which is formed by the acid-catalyzed hydrolysis of inulin (Scheme 1), increases significantly by feeding H_2 with a low pressure (0.2 MPa). A further increase in the H_2 pressure increased the yields of sorbitol and mannitol owing to the occurrence of hydrogenation of fructose or other intermediates at higher H_2 pressures. When H_2 pressure increased from 2 to 4 MPa, the yield of hexitols increased from 52% to 59%, while that of fructose decreased from 17% to 13%. Beside fructose, a part of oligomers, which were produced by the partial hydrolysis of inulin, may also contribute to the formation of hexitols under higher H_2 pressures.

The loading of Ru is another key factor for the efficient conversion of inulin. As displayed in Fig. 6, without loading Ru, the $Cs_3PW_{12}O_{40}$ was less active for the conversion of inulin even under H_2 atmosphere (inulin conversion < 10%). The conversion of inulin increased to ~100% after loading a small amount of Ru (0.2 wt%) onto the $Cs_3PW_{12}O_{40}$. Meanwhile, the introduction of a small amount of Ru significantly enhanced the yield of fructose, the hydrolysis product. At higher loadings of Ru, the yields of sorbitol and mannitol increased at the expense of that of fructose due to the hydrogenation catalyzed by Ru nanoparticles.

In short, the results described above suggest that new acid sites effective for the hydrolysis of inulin to fructose are generated over the $Ru/Cs_3PW_{12}O_{40}$ catalyst. The presence of H_2 and the loading of Ru play crucial roles in the generation of such acid sites. These generated acid sites are believed to be responsible for the superior activity of the $Ru/Cs_3PW_{12}O_{40}$ catalyst, which does not possess intrinsic Brønsted acidity, for the conversion of inulin or cellulose into hexitols. Under a lower H_2 pressure or over the catalyst with a lower Ru loading, the formation of fructose can be significantly promoted because of the accelerated hydrolysis ability and the relatively lower hydrogenation ability under such circumstances.

3.5 Characterizations of Brønsted acid sites generated in the presence of H_2 over the $Ru/Cs_3PW_{12}O_{40}$ catalyst

To gain direct evidence for the generation of the Brønsted acid sites in the presence of H_2, we have performed FT-IR spectroscopic studies of adsorbed pyridine. In these studies, the $Ru/Cs_3PW_{12}O_{40}$ catalyst was pretreated in an *in situ* IR cell under H_2 at 573 K for 1 h, followed by evacuation at the same temperature. Then, the $Ru/Cs_3PW_{12}O_{40}$ catalyst was exposed to pyridine at 423 K for 0.5 h. After cooling down to 303 K followed by a brief evacuation, H_2 was introduced into the *in situ* IR cell. In the absence of H_2, an IR band at 1425–1450 cm^{-1} was observed. This band could be ascribed to the pyridine adsorbed on Lewis

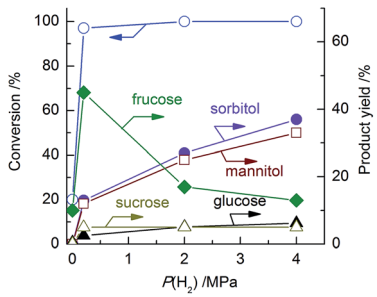

Fig. 5 Effect of H_2 pressure on catalytic behaviours of the $Ru/Cs_3PW_{12}O_{40}$ catalyst for the conversion of inulin in water under H_2. Reaction conditions: inulin, 0.2 g; catalyst (Ru loading, 1.0 wt%), 0.020 g; H_2O, 10 mL; $T = 363$ K; $t = 4$ h.

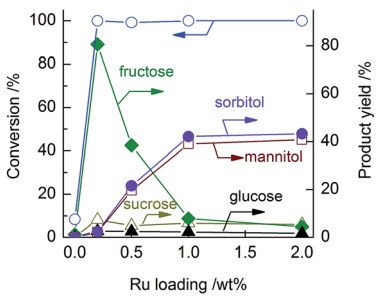

Fig. 6 Effect of Ru loading on catalytic behaviours of the $Ru/Cs_3PW_{12}O_{40}$ catalyst for the conversion of inulin in water under H_2. Reaction conditions: inulin, 0.20 g; catalyst, 0.050 g; H_2O, 10 mL; H_2, 2 MPa; $T = 363$ K; $t = 4$ h.

acid sites.[25] The introduction of H_2 decreased the IR band at 1450 cm^{-1} and resulted in a significant increase in the IR band at 1540 cm^{-1} (Fig. 7A). This IR band could be assigned to the pyridine adsorbed on the Brønsted acid sites.[25] The intensity of the IR band at 1540 cm^{-1} increased with the H_2 pressure, suggesting the generation of the Brønsted acid sites under H_2. When N_2 was introduced into the IR cell instead of H_2, the IR band at 1540 cm^{-1} was not enhanced (Fig. 7B), confirming that the Brønsted acid sites were originated from H_2. We also performed the pyridine-adsorbed FT-IR studies for the $Cs_3PW_{12}O_{40}$ sample without Ru. The IR band at 1540 cm^{-1} was not enhanced in the presence of H_2 (Fig. S8†). This provides evidence that Ru nanoparticles are essential for the generation of Brønsted acid sites over the $Ru/Cs_3PW_{12}O_{40}$ under H_2 atmosphere. Actually, many recent studies have demonstrated that Ru nanoparticles can activate H_2 under mild conditions.[26] Furthermore, we carried out the same study for the Ru/Al_2O_3 catalyst. The IR band at 1540 cm^{-1} ascribed to the Brønsted acid sites could not be observed over the Ru/Al_2O_3 in the presence of H_2 (Fig. S9†). It is noteworthy that the formation of protons from H_2 was once proposed over a Pt/Al_2O_3 catalyst *via* a spillover effect in an early study.[8a] However, we could not observe the generation of the Brønsted acid sites from H_2 over our Ru/Al_2O_3. Therefore, the $Ru/Cs_3PW_{12}O_{40}$ is a quite unique system for the generation of Brønsted acid sites in the presence of H_2.

It is expected that one electron will be released simultaneously with the generation of one proton, the Brønsted acid site, from the hydrogen species over the $Ru/Cs_3PW_{12}O_{40}$ catalyst. To gain further information on this process, we have monitored the structure change of the catalyst by Raman spectroscopic measurements. Fig. 8 shows the Raman spectra of the $Ru/Cs_3PW_{12}O_{40}$ catalyst under N_2 and H_2 atmospheres at 423 K. Under N_2 atmosphere, Raman bands at 1002, 990, 897, 548, and ~240 cm^{-1} were observed. These bands could be attributed to the strong W=O symmetric and asymmetric stretching modes (1002 and 990 cm^{-1}), the asymmetric stretching vibration of bridging $W–O_b–W$ (O_b denotes a corner sharing bridging oxygen atom) (897 cm^{-1}), the symmetric stretching of bridging $W–O_c–W$ (O_c denotes an edge-sharing bridging oxygen atom) (548 cm^{-1}), and the bending mode of the bridging W–O–W bonds of the intact Keggin structure (~240 cm^{-1}).[27] When the gas atmosphere was switched from N_2 to H_2, all these major bands attributable to Keggin unit still remained (Fig. 8A). However, a shift of W=O stretching vibration bands to higher wavenumbers was observed (Fig. 8B), suggesting a perturbation of W=O bonds in the primary Keggin structure in the presence of H_2. It is noteworthy that the W=O stretching vibration bands shift back after H_2 was replaced by N_2. In other words, the shifts of Raman bands are reversible. On the other hand, no such shifts of Raman bands were observed by switching the atmosphere from N_2 to H_2 for $Cs_3PW_{12}O_{40}$ alone (Fig. S10†). These results suggest that the shift of the Raman bands belonging to the W=O stretching vibrations is related to the generation of Brønsted acidity. We speculate that the electrons released during the formation of protons from hydrogen species might migrate to $Cs_3PW_{12}O_{40}$, and the reduction of tungsten species may cause the shift of Raman bands belonging to W=O stretching vibrations.

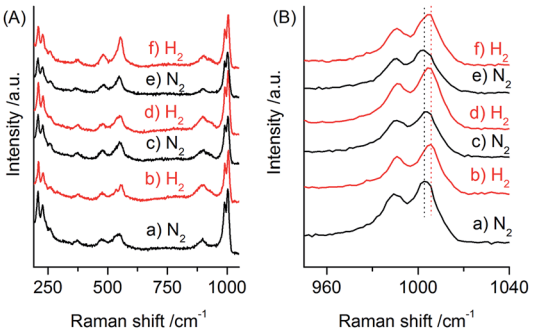

Fig. 8 Raman spectra for the $Ru/Cs_3PW_{12}O_{40}$ under N_2 and H_2 atmospheres at 423 K. (A) 200–1040 cm^{-1}, (B) 940–1040 cm^{-1}. (a) After the introduction of N_2 into the pretreated sample, (b) 10 min after switching to H_2, (c) 10 min after switching again to N_2, (d) 10 min after switching again to H_2, (e) 10 min after switching again to N_2, (f) 10 min after switching again to H_2.

We further performed ESR spectroscopic studies for the $Ru/Cs_3PW_{12}O_{40}$ catalyst in the presence of H_2. An ESR signal appeared at ~3700 G after contact of the sample with H_2 at 423 K (Fig. 9). This signal could be attributed to W^{5+}.[28] The ESR signal disappeared when H_2 was purged and replaced by N_2. The appearance of W^{5+} in the presence of H_2 provides further evidence that the released electrons are transferred to $Cs_3PW_{12}O_{40}$ and are stored in the tungsten species.

Actually, the concept of generation of new Brønsted acid sites from molecular H_2 has been proposed by Hattori and co-workers for a few metal oxide-supported transition metal catalysts such as $Pt/SO_4^{2-}–ZrO_2$.[29] These acid sites are reversible and can only appear under H_2 atmosphere. Such a kind of Brønsted acidity has found applications in the hydroisomerization of alkanes.[29] Based on our present studies described above and the model suggested by Hattori and co-workers, we have proposed a mechanism for the generation of Brønsted acid sites on our $Ru/Cs_3PW_{12}O_{40}$ catalyst (Scheme 2). In brief, molecular H_2 is first dissociated on Ru nanoparticles, and then, the formed atomic H species spill over to the $Cs_3PW_{12}O_{40}$ surface. The H atom may

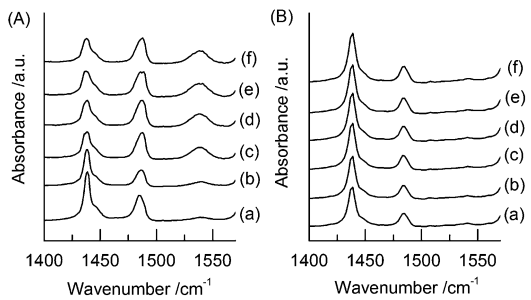

Fig. 7 Pyridine-adsorbed FT-IR spectra for the $Ru/Cs_3PW_{12}O_{40}$ under H_2 (A) and N_2 (B) atmospheres with different pressures. (a) At 323 K after pretreatment in H_2 at 573 K followed by evacuation, (b) under 13 kPa H_2 or N_2, (c) under 19 kPa H_2 or N_2, (d) under 26 kPa H_2 or N_2, (e) under 33 kPa H_2 or N_2, (f) under 45 kPa H_2 or N_2.

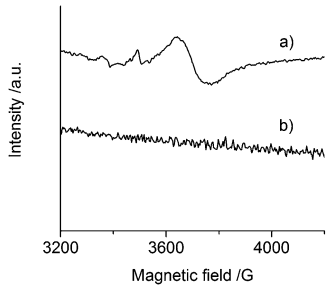

Fig. 9 ESR spectra of the Ru/$Cs_3PW_{12}O_{40}$ catalyst. (a) After contact with H_2 at 423 K. (b) After contact with H_2 at 423 K, followed by purging with N_2.

release one electron, resulting in the formation of Brønsted acid site (proton) on the $Cs_3PW_{12}O_{40}$ surface. Meanwhile, a small fraction of tungsten species on $Cs_3PW_{12}O_{40}$ is reduced to W^{5+}. Our experimental results indicate that these processes are reversible. Thus, the proton may recombine one electron from W^{5+}, forming atomic H species. The reverse spill-over of the H species to Ru nanoparticles occurs subsequently, leading to the formation of molecular H_2. In the presence of a reactant, the reversibly generated protons can catalyze the hydrolysis reaction. The co-existence of protons (Brønsted acid sites) and H atoms on catalyst surfaces leads to synergistic effects for the conversion of inulin to hexitols.

3.6 Size effects of Ru nanoparticles on catalytic conversion of inulin

It is known that the size of metal nanoparticles plays crucial roles in their catalytic behaviours in many reactions.[30] To investigate the size effect of Ru nanoparticles in our system, we have synthesized colloidal Ru nanoparticles with four different mean sizes (1.6, 2.7, 5.0, and 10.8 nm) by changing the reduction temperature and the aging time during the reduction of $RuCl_3$ with ascorbic acid. Table 3 shows the conditions used for the synthesis of colloids and the obtained mean sizes of Ru nanoparticles derived from TEM measurements (Fig. S11†). The increase in the reduction temperature increased the mean size of Ru nanoparticles. This is possibly because a higher reduction temperature may increase the probability of collision among the particles during the particle growing process, leading to larger Ru nanoparticles. A longer aging time also resulted in a larger mean size of colloidal Ru nanoparticles due to the Ostwald ripening, which was caused by the dissolved smaller particles precipitating onto the larger particles.[31]

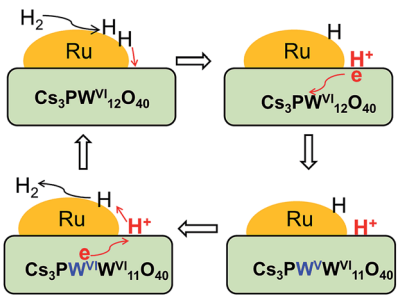

Scheme 2 Proposed mechanism for the generation of Brønsted acid sites over the Ru/$Cs_3PW_{12}O_{40}$ catalyst in the presence of H_2.

Then, the colloidal Ru nanoparticles were loaded onto the $Cs_3PW_{12}O_{40}$. We measured the dispersion of Ru particles over each supported catalyst by CO chemisorption, and estimated the size of Ru particles using the dispersion as mentioned above. The sizes of Ru nanoparticles estimated from Ru dispersions over these catalysts are close to those in the colloidal precursors estimated by TEM except for the catalyst with the largest mean size of Ru particles (Table 3).

Fig. 10 shows the catalytic performances of the Ru/$Cs_3PW_{12}O_{40}$ catalysts with different mean sizes of Ru particles for the conversion of inulin in water under H_2 atmosphere. Fructose and hexitols (sorbitol and mannitol) were major products. Small amounts of sucrose and glucose were also formed. Over the catalyst with smaller Ru nanoparticles, inulin was mainly transformed into hexitols. A hexitol yield of 84% was attained after a reaction at 363 K for 4 h by using the catalyst with a mean Ru particle size of 1.9 nm. Upon increasing the mean size of Ru particles from 1.9 to 27 nm, the yield of hexitols gradually decreased, while that of fructose increased gradually. The fructose yield increased from 4.9% to 75% with an increase in the mean size of Ru particles from 1.9 to 13 nm. It should be noted that the conversion of inulin over the $Cs_3PW_{12}O_{40}$ without Ru provided fructose with a yield of <5%. It is quite interesting that the size of Ru nanoparticles determines the product selectivities. By regulating the size of Ru nanoparticles, the product distributions can be tuned.

To gain further insights into the Ru particle size effect on the reaction pathways, we have investigated the time courses for the conversions of inulin over the Ru/$Cs_3PW_{12}O_{40}$ catalysts with different mean Ru particle sizes. Fig. 11 shows that the catalysts with smaller Ru particles provide higher inulin conversions at a short reaction time. After reaction for 1 h, inulin could be completely converted over the catalyst with a mean Ru particle size of 1.9 nm, whereas only ~60% of inulin conversion was attained on the catalyst with a mean Ru particle size of 27 nm. Thus, the catalyst with a smaller mean size of Ru nanoparticles was more active for the transformation of inulin. Fructose was formed as the major product at the initial reaction stage irrespective of the mean size of Ru particles in the catalyst. For the catalysts with mean Ru particle sizes of 1.9, 2.3 and 6.0 nm, the prolonging of the reaction time decreased the yield of fructose and increased those of sorbitol and mannitol (Fig. 11A–C). This observation confirms that sorbitol and mannitol are formed by the hydrogenation of fructose, which is the reaction intermediate, over these catalysts. On the other hand, for the Ru/$Cs_3PW_{12}O_{40}$ catalyst with a mean Ru particle size of 27 nm (Fig. 11D), the yields of hexitols (sorbitol and mannitol) were very low (<8%) even after 6 h of reaction. The yield of fructose increased to ~80% after 6 h of reaction over this catalyst. Thus, the hydrogenation of fructose proceeded very slowly over the catalyst with a larger mean Ru particle size.

We further studied the effect of Ru particle size on catalytic behaviours of the Ru/$Cs_3PW_{12}O_{40}$ catalysts for the

Table 3 Mean sizes and dispersion of Ru particles in colloidal precursors or over the $Cs_3PW_{12}O_{40}$-supported catalysts

Conditions used for colloid synthesis	Ru size in colloids[a] (nm)	Ru dispersion[b]	Ru size in catalyst[c] (nm)
Reduction temp., 353 K; aging time, 1 h; solvent, water	1.6	0.49	1.9
Reduction temp., 353 K; aging time, 12 h; solvent, water	2.7	0.40	2.3
Reduction temp., 383 K; aging time, 0.5 h; solvent, 60% ethylene glycol	5.0	0.15	6.0
Reduction temp., 383 K; aging time, 12 h; solvent, 60% butylene glycol	10.8	0.033	27

[a] Evaluated from TEM micrographs (Fig. S11). [b] Measured from CO chemisorption for $Ru/Cs_3PW_{12}O_{40}$. [c] Calculated from Ru dispersion.

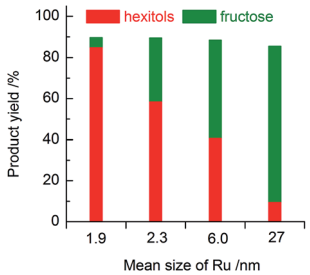

Fig. 10 Catalytic behaviours of the $Ru/Cs_3PW_{12}O_{40}$ catalysts with different mean sizes of Ru nanoparticles for the conversion of inulin in water under H_2. Reaction conditions: inulin, 0.20 g; $Ru/Cs_3PW_{12}O_{40}$, 0.050 g; H_2O, 10 mL; H_2, 2 MPa; $T = 363$ K; $t = 4$ h.

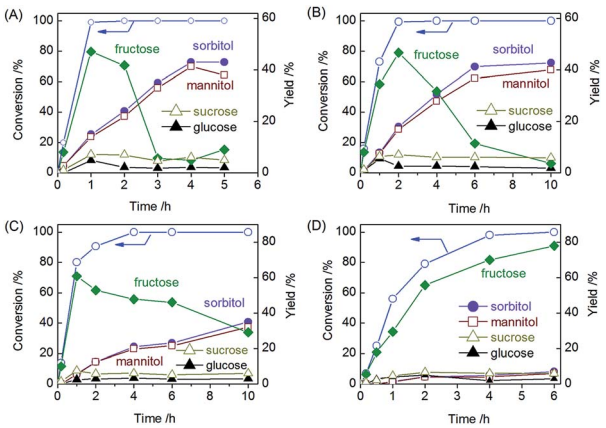

Fig. 11 Time courses for conversion of inulin over the $Ru/Cs_3PW_{12}O_{40}$ catalysts with different mean Ru particle sizes (A) 1.9 nm, (B) 2.3 nm, (C) 6.0 nm, (D) 27 nm. Reaction conditions: inulin, 0.20 g; $Ru/Cs_3PW_{12}O_{40}$, 0.050 g; H_2O, 10 mL; H_2, 2 MPa; $T = 363$ K.

hydrogenation of fructose. The major products in the hydrogenation of fructose were hexitols (sorbitol and mannitol) and the selectivity to hexitols was >98% over the $Ru/Cs_3PW_{12}O_{40}$ catalyst irrespective of the mean Ru particle size. However, the conversion of fructose was strongly dependent on the size of Ru particles (Fig. S12†). We evaluated the rates of fructose conversions over the catalysts with different mean Ru particle sizes by using the conversions at the initial reaction stage. The results are summarized in Table 4. We also calculated the turnover frequency (TOF), *i.e.*, the moles of fructose converted per unit time at the initial stage per mole of surface Ru atoms. The TOF for the hydrogenation of fructose to hexitols increased sharply with decreasing the mean size of Ru particles from 6 nm to 1.9 nm (Fig. S13†). This result suggests that the hydrogenation of fructose over the $Ru/Cs_3PW_{12}O_{40}$ catalyst is a structure-sensitive reaction.

For comparison, the initial rates of inulin conversions over the $Ru/Cs_3PW_{12}O_{40}$ catalysts with different Ru particle sizes were also evaluated using the conversions at a shorter reaction time (0.17 h) in Fig. 11. The hydrolysis product, *i.e.*, fructose, was mainly formed at such a shorter reaction time. It should be noted that the hydrolysis of inulin proceeded very slow over the $Cs_3PW_{12}O_{40}$ alone without loading Ru particles. Thus, the presence of Ru nanoparticles plays a pivotal role in the hydrolysis of inulin in our system. As displayed in Table 4, the rate of inulin hydrolysis also depended on the mean size of Ru particles; the smaller mean Ru particle size afforded a higher rate of inulin hydrolysis. This can be interpreted by our proposed model that the Brønsted acid sites for hydrolysis of inulin are generated from H_2 on Ru nanoparticles (Scheme 2). We speculate that the smaller Ru particles, which contain higher fractions of coordinatively unsaturated Ru sites, favour the dissociation of H_2 to atomic hydrogen species. Thus, the catalyst with smaller Ru particles can generate higher concentrations of Brønsted acid sites over catalyst surfaces for the hydrolysis reaction.

However, the dependence of the rate of inulin hydrolysis on the Ru particle size is less strong than that of fructose hydrogenation. A comparison of the date in Table 4 reveals that, for the catalyst with a larger mean size of Ru nanoparticles (particularly, 27 nm), the rate of inulin hydrolysis is higher than that of fructose hydrogenation. This can explain the observation that fructose is formed as the dominant product over the catalyst with a mean Ru particle size of 27 nm even after a long-time

Table 4 Effect of mean size of Ru nanoparticles on the rates of inulin hydrolysis and fructose hydrogenation over the $Ru/Cs_3PW_{12}O_{40}$ catalysts

Mean Ru size (nm)	Initial reaction rate (mmol g_{cat}^{-1} h^{-1})	
	Fructose hydrogenation[a]	Inulin hydrolysis[b]
1.9	117	30
2.3	72	23
6.0	13	20
27	1	10

[a] Catalyst, 0.050 g; fructose, 0.20 g; H_2O, 10 mL; H_2, 2 MPa; $T = 363$ K. [b] Catalyst, 0.050 g; inulin, 0.20 g; H_2O, 10 mL; H_2, 2 MPa; $T = 363$ K.

reaction (Fig. 11D). Upon decreasing the mean size of Ru nanoparticles, the rate of fructose hydrogenation increased more rapidly. As a result, the rate of fructose hydrogenation exceeded that of inulin hydrolysis over the catalysts with smaller Ru nanoparticles. In other words, the rate-determining step changed from the fructose hydrogenation to inulin hydrolysis with decreasing the mean size of Ru nanoparticles over the Ru/$Cs_3PW_{12}O_{40}$ catalysts. Thus, it becomes understandable that hexitols are produced as the main products over the catalyst with a smaller mean size of Ru particles (in particular 1.9 or 2.3 nm), while fructose is formed dominantly over the one with bigger Ru particles.

4. Conclusion

Ru nanoparticles loaded on the Keggin-type polyoxometalates, *i.e.*, Ru/$Cs_xH_{3-x}PW_{12}O_{40}$, were highly efficient for the conversions of inulin and cellulose into hexitols in water in the presence of H_2. The Ru/$Cs_xH_{3-x}PW_{12}O_{40}$ catalysts exhibited significantly higher yields of hexitols than the Ru catalysts loaded on other solid acids such as Al_2O_3, HZSM-5 and MCM-22. It is unexpected that the Ru/$Cs_3PW_{12}O_{40}$ catalyst, which does not possess strong intrinsic Brønsted acidity, exhibits superior performances for the conversions of both inulin and cellulose into hexitols. Hexitol yields of 84% and 45% were achieved for the conversions of inulin and cellulose over the Ru/$Cs_3PW_{12}O_{40}$ catalyst at 363 K for 4 h and 433 K for 24 h, respectively. This catalyst was robust during the recycling uses. We have demonstrated that new Brønsted acid sites can be generated over the Ru/$Cs_3PW_{12}O_{40}$ catalyst from molecular H_2. Through characterizations by pyridine-adsorbed FT-IR, Raman, and ESR spectroscopic measurements, we propose that molecular H_2 is first dissociated on Ru particles, and then, the H atoms spillover to the $Cs_3PW_{12}O_4$ surface, which are subsequently converted to protons by releasing electrons to the support. The H_2-originated Brønsted acid sites are reversible and responsible for the superior catalytic performance of the Ru/$Cs_3PW_{12}O_4$ catalyst.

We further found that the mean size of Ru nanoparticles over the Ru/$Cs_3PW_{12}O_{40}$ catalyst exerted significant effects on the products distribution in the conversion of inulin in water under H_2 atmosphere. For the catalyst with a larger mean size of Ru nanoparticles (27 nm), fructose, a hydrolysis product, was attained as the major product, whereas the catalysts with smaller Ru nanoparticles afforded hexitols with higher yields. The rates of both inulin hydrolysis and fructose hydrogenation were dependent on the mean size of Ru particles, and smaller Ru particles favoured the reaction rates for both steps. The rate of fructose hydrogenation increased more significantly upon decreasing the mean Ru particle size, and the rate determining step changed from fructose hydrogenation to inulin hydrolysis at the same time.

Acknowledgements

This work was supported by the National Natural Science Foundation of China (no. 21173172, 21103143, and 21033006), the Research Fund for the Doctorial Program of Higher Education (no. 20130121130001), and the Program for Changjiang Scholars and Innovative Research Team in Chinese Universities (no. IRT1036).

Notes and references

1 (*a*) D. Klemm, B. Heublein, H. P. Fink and A. Bohn, *Angew. Chem., Int. Ed.*, 2005, **44**, 3358; (*b*) P. L. Dhepe and A. Fukuoka, *ChemSusChem*, 2008, **1**, 969; (*c*) S. Van de Vyver, J. Geboers, P. A. Jacobs and B. F. Sels, *ChemCatChem*, 2011, **3**, 82; (*d*) C. H. Zhou, X. Xia, C. X. Lin, D. S. Tong and J. Beltramini, *Chem. Soc. Rev.*, 2011, **40**, 5588; (*e*) W. Deng, Y. Wang, Q. Zhang and Y. Wang, *Catal. Surv. Asia*, 2012, **16**, 91; (*f*) H. Kobayashi and A. Fukuoka, *Green Chem.*, 2013, **15**, 1740; (*g*) M. Yabushita, H. Kobayashi and A. Fukuoka, *Appl. Catal., B*, 2014, **145**, 1; (*h*) A. Wang and T. Zhang, *Acc. Chem. Res.*, 2013, **46**, 1377.

2 S. J. Kays and S. F. Nottingham, *Biology and Chemistry of Jerusalem Artichoke: Helianthus Tuberosus L.*, CRC Press, Boca Raton, 2007.

3 (*a*) A. W. Heinen, G. Papadogianakis, R. A. Sheldon, J. A. Peters and H. van Bekkum, *J. Mol. Catal.*, 1999, **142**, 17; (*b*) A. W. Heinen, J. A. Peters and H. van Bekkum, *Carbohydr. Res.*, 2001, **330**, 381.

4 L. Zhou, A. Wang, C. Li, M. Zheng and T. Zhang, *ChemSusChem*, 2013, **5**, 932.

5 T. Werpy and G. Petersen, *Top Value Added Chemicals from Biomass*, 2004, vol. 1, pp. 58–60, http://www.pnl.gov/main/publications/external/technical_reports/PNNL-14808.pdf.

6 C. Luo, S. Wang and H. Liu, *Angew. Chem., Int. Ed.*, 2007, **46**, 7636.

7 (*a*) R. Palkovits, K. Tajvidi, J. Procelewska, R. Rinaldi and A. Ruppert, *Green Chem.*, 2010, **12**, 972; (*b*) J. Geboers, S. Van de Vyver, K. Carpentier, P. Jacobs and B. Sels, *Chem. Commun.*, 2011, **47**, 5590; (*c*) G. Liang, C. Wu, L. He, J. Ming, H. Cheng, L. Zhuo and F. Zhao, *Green Chem.*, 2011, **13**, 839.

8 (*a*) A. Fukuoka and P. L. Dhepe, *Angew. Chem., Int. Ed.*, 2006, **45**, 5161; (*b*) H. Kobayashi, H. Matsuhashi, T. Komanoya, K. Hara and A. Fukuoka, *Chem. Commun.*, 2011, **47**, 2366.

9 (*a*) W. P. Deng, X. S. Tan, W. H. Fang, Q. H. Zhang and Y. Wang, *Catal. Lett.*, 2009, **133**, 167; (*b*) W. Deng, M. Liu, X. Tan, Q. Zhang and Y. Wang, *J. Catal.*, 2010, **271**, 22.

10 (*a*) S. Van de Vyver, J. Geboers, W. Schutyser, M. Dusselier, P. Eloy, E. Dornez, J. W. Seo, C. M. Courtin, E. M. Gaigneaux, P. A. Jacobs and B. F. Sels, *ChemSusChem*, 2012, **5**, 1549; (*b*) P. Yang, H. Kobayashi, K. Hara and A. Fukuoka, *ChemSusChem*, 2012, **5**, 920; (*c*) H. Kobayashi, Y. Hosaka, K. Hara, B. Feng, Y. Hirosaki and A. Fukuoka, *Green Chem.*, 2014, **16**, 637.

11 W. Deng, Q. Zhang and Y. Wang, *Dalton Trans.*, 2012, **41**, 9817.

12 (*a*) K. Shimizu, H. Furukawa, N. Kobayashi, Y. Itaya and A. Satusma, *Green Chem.*, 2009, **11**, 1627; (*b*) J. Tian, J. Wang, S. Zhao, C. Jiang, X. Zhang and X. Wang, *Cellulose*, 2010, **17**, 587; (*c*) Y. Ogasawara, S. Itagaki,

K. Yamaguchi and N. Mizuno, *ChemSusChem*, 2011, **4**, 519; (*d*) J. Tian, C. Fan, M. Cheng and X. Wang, *Chem. Eng. Technol.*, 2011, **34**, 482.

13 (*a*) J. Geboers, S. Van de Vyver, K. Carpentier, K. de Blochouse, P. Jacobs and B. Sels, *Chem. Commun.*, 2010, **46**, 3577; (*b*) R. Palkovits, K. Tajvidi, A. M. Ruppert and J. Procelewska, *Chem. Commun.*, 2011, **47**, 576.

14 J. Chen, S. Wang, J. Huang, L. Chen, L. Ma and X. Huang, *ChemSusChem*, 2013, **6**, 1545.

15 T. Okuhara, *Chem. Rev.*, 2002, **102**, 3641.

16 J. Geboers, S. Van de Vyver, K. Carpentier, P. Jacobs and B. Sels, *Green Chem.*, 2011, **13**, 2167.

17 M. Liu, W. Deng, Q. Zhang, Y. Wang and Y. Wang, *Chem. Commun.*, 2011, **47**, 9717.

18 M. Langpape, J. M. M. Millet, U. S. Ozkan and M. Boudeulle, *J. Catal.*, 1999, **181**, 80.

19 J. Zhang, M. Sun, C. Cao, Q. Zhang, Y. Wang and H. Wan, *Appl. Catal., A*, 2010, **380**, 87.

20 B. M. Faroldi, E. A. Lombardo and L. M. Cornaglia, *Appl. Catal., A*, 2009, **369**, 15.

21 A. W. Heinen, J. A. Peters and H. van Bekkum, *Carbohydr. Res.*, 2000, **328**, 449.

22 N. Essayem, G. Coudurier, M. Fournier and J. C. Védrine, *Catal. Lett.*, 1995, **34**, 223.

23 T. Nakato, M. Kimura, S. Nakata and T. Okuhara, *Langmuir*, 1998, **14**, 319.

24 D. An, A. Ye, W. Deng, Q. Zhang and Y. Wang, *Chem.–Eur. J.*, 2012, **18**, 2938.

25 M. I. Zaki, M. A. Hasan, F. A. Al-Sagheer and L. Pasupulety, *Colloids Surf., A*, 2001, **190**, 261.

26 (*a*) C. Hubert, A. Denicourt-Nowicki, A. Roucoux, D. Landy, B. Leger, G. Crowyn and E. Monflier, *Chem. Commun.*, 2009, 1228; (*b*) M. Zahmakıran, Y. Tonbul and S. Özkar, *J. Am. Chem. Soc.*, 2010, **132**, 6541; (*c*) N. Steinfeldt, M. Sebek and K. Jänisch, *J. Catal.*, 2012, **289**, 249.

27 L. Nakka, J. E. Molinari and I. E. Wachs, *J. Am. Chem. Soc.*, 2009, **131**, 15544.

28 (*a*) L. Bih, L. Abbas, M. Azrour, Y. E. Amraoui and A. Nadiri, *J. Therm. Anal. Calorim.*, 2005, **81**, 57; (*b*) D. Boudlich, L. Bih, M. E. H. Archidi, M. Haddad, A. Yacoubi, A. Nadiri and B. Elouadi, *J. Am. Ceram. Soc.*, 2002, **85**, 623.

29 (*a*) H. Hattori and T. Shishido, *Catal. Surv. Jpn.*, 1997, **1**, 205; (*b*) H. Hattori, *Top. Catal.*, 2010, **53**, 432.

30 Q. Zhang, W. Deng and Y. Wang, *Chem. Commun.*, 2011, **47**, 9275.

31 W. Fang, J. Chen, Q. Zhang and Y. Wang, *Chem.–Eur. J.*, 2011, **17**, 1247.